PNNL-23995

Pacific Northwest
NATIONAL LABORATORY

Proudly Operated by **Battelle** *Since 1965*

Testing of the KRI-developed Silicon PIN Radioxenon Detector

January 2015

MP Foxe
JI McIntyre

U.S. DEPARTMENT OF
ENERGY

Prepared for the U.S. Department of Energy
under Contract **DE-AC05-76RL01830**

PACIFIC NORTHWEST NATIONAL LABORATORY
operated by
BATTELLE
for the
UNITED STATES DEPARTMENT OF ENERGY
under Contract DE-AC05-76RL01830

Printed in the United States of America

Available to DOE and DOE contractors from the
Office of Scientific and Technical Information,
P.O. Box 62, Oak Ridge, TN 37831-0062;
ph: (865) 576-8401
fax: (865) 576-5728
email: reports@adonis.osti.gov

Available to the public from the National Technical Information Service
5301 Shawnee Rd., Alexandria, VA 22312
ph: (800) 553-NTIS (6847)
email: orders@ntis.gov <http://www.ntis.gov/about/form.aspx>
Online ordering: http://www.ntis.gov

This document was printed on recycled paper.
(8/2010)

PNNL-23995

Testing of the KRI-developed Silicon PIN Radioxenon Detector

MP Foxe
JI McIntyre

January 2015

Prepared for
the U.S. Department of Energy
under Contract DE-AC05-76RL01830

Pacific Northwest National Laboratory
Richland, Washington 99352

Executive Summary

Radioxenon detectors are used for the verification of the Comprehensive Nuclear-Test-Ban Treaty in a network of detectors located throughout the world known as the International Monitoring System (IMS). The Comprehensive Nuclear-Test-Ban Treaty Organization Provisional Technical Secretariat has tasked Pacific Northwest National Laboratory (PNNL) with testing a V.G. Khlopin Radium Institute (KRI) and Lares Ltd.-developed silicon p-type–intrinsic–n-type (PIN) detector for radioxenon detection. PNNL measured radioxenon with the silicon PIN detector and determined its potential compared to current plastic scintillator beta cells. The PNNL-tested silicon detector experienced noise issues, but a second detector that was tested in Russia at Lares Ltd. did not exhibit the noise issues. Without the noise issues, the silicon detector produces much better energy resolution and isomer peak separation than a conventional plastic scintillator cell used in the Swedish Automatic Unit for Noble Gas Acquisition (SAUNA) systems in the IMS.

Under the assumption of 1 cm^3 of xenon in laboratory-like conditions, 24-hour count time (12-hour count time for the SAUNA), with the respective shielding the minimum detectable concentrations for the silicon detector tested by Lares Ltd. (and a conventional SAUNA system) were calculated to be:

- ^{131}mXe – 0.12 mBq/m^3 (0.12 mBq/m^3)
- ^{133}Xe – 0.18 mBq/m^3 (0.21 mBq/m^3)
- ^{133m}Xe – 0.07 mBq/m^3 (0.15 mBq/m^3)
- ^{135}Xe – 0.45 mBq/m^3 (0.67 mBq/m^3)

Detection limits, which are one of the important factors in choosing the best detection technique for radioxenon in field conditions, are significantly better for the silicon PIN detector than for SAUNA-like detection systems for ^{131m}Xe and ^{133m}Xe, but detection limits are similar for ^{133}Xe and ^{135}Xe.

Another important factor is the amount of "memory effect" or carry-over signal from one radioxenon measurement to the subsequent sample. The memory effect is reduced by a factor of 10 in the silicon PIN detector compared to the current plastic scintillator cells. There is potential for further reduction with the removal of plastics within the cell, which will need to be explored in future work.

A third important parameter in choosing the best detection technique for radioxenon is the resolution of the electron detection. While the resolution is important in determining the minimum detectable concentration, it plays a larger role in source identification when there is a visible signal. The silicon PIN diodes generated improved resolution over a similar plastic scintillator cell. With the improved resolution, it becomes easier to distinguish the radioxenon isomers (^{133m}Xe and ^{131m}Xe) from the ^{133}Xe beta continuum background. With the beta background from ^{133}Xe ever present with the detection of the isomers, the improved resolution proves vital in calculating the ratios of the three isotopes. The anthropogenic sources of radioxenon (medical isotope production and nuclear reactors) are more accurately distinguished with an accurate measurement of the isotopic ratios.

Based on the results documented in this report, a silicon PIN beta cell shows the potential to aid in the operation and discriminating power of the IMS for the Comprehensive Nuclear-Test-Ban Treaty

Organization. However, a number of issues need attention before a detector of this design would be reliable enough for field operations in the IMS, including (but not limited to)

- studying the robustness of the design in field conditions
- eliminating or minimizing the noise and variability of individual silicon detector elements
- understanding the long-term gain stability of the Si detectors
- reducing the non-silicon materials within the cell (i.e., the plastic housing).

Acronyms and Abbreviations

CTBT	Comprehensive Nuclear-Test-Ban Treaty
CTBTO	Comprehensive Nuclear-Test-Ban Treaty Organization
IMS	International Monitoring System
KRI	V.G. Khlopin Radium Institute
MDC	minimum detectable concentration
NaI	sodium iodide
PIN	p-type – intrinsic – n-type
PNNL	Pacific Northwest National Laboratory
QA/QC	quality assurance/quality control
SAUNA	Swedish Automatic Unit for Noble gas Acquisition

Contents

Figures

1.0 Introduction

The International Monitoring System (IMS) is a network of systems to collect and measure airborne debris around the world to monitor for nuclear explosions as part of the verification regime of the Comprehensive Nuclear-Test-Ban Treaty (CTBT). One technology the IMS employs is radioxenon detectors. In the radioxenon detectors, xenon gas is injected into a plastic scintillator beta cell (e.g., BC-404) to detect the electrons emitted, and the gamma rays are detected by a surrounding sodium iodide (NaI) detector.

The radioxenon systems focus on four xenon isotopes of interest: ^{131m}Xe, ^{133m}Xe (the products of medical isotope production), and ^{133}Xe and ^{135}Xe (potential products of a nuclear explosion). Good detector resolution is critical to distinguishing between ^{131m}Xe, ^{133m}Xe, and ^{133}Xe. ^{131m}Xe and ^{133m}Xe both emit conversion electrons within the ^{133}Xe beta continuum (McIntyre et al. 2001). Current plastic scintillator beta cells have a resolution of approximately 30 percent at 129 keV, the energy of the ^{131m}Xe conversion electron. There have been efforts to build a beta cell using silicon detectors capable of resolutions of approximately 5 percent for the 129-keV conversion electron peak (Cagniant et al. 2014, Le Petit et al. 2013, Schroettner et al. 2010), but none have replaced the current radioxenon detectors.

Lares Ltd. has developed a six-sided beta cell, with a 1.68-cm × 1.68-cm silicon p-type–intrinsic–n-type (PIN) diode detector on each side of the cube. The 8.1-cm^3 cell is housed inside of a 6.3-cm × 6.3-cm thallium-doped sodium iodide (NaI(Tl)) detector (shown in Figure 1.1), which is surrounded by approximately 50 kg of lead. PNNL has been tasked with testing the performance of the silicon PIN detector and determining whether its capabilities meet the Comprehensive Nuclear-Test-Ban Treaty Organization (CTBTO) verification standards. In this report, we present the results of the operation of the silicon PIN detector, which was tested along with plastic scintillator beta cells and a similar silicon PIN detector for comparison.

Figure 1.1. Detector Setup with the Beta Cell Formed out of Six Silicon Detectors Placed Inside the Well of an NaI Detector

2.0 Experiment Overview

The beta cell was fabricated from six silicon PIN diodes housed in a plastic holder. Each silicon PIN diode is 0.6-mm thick, and biased to 20 V. The NaI detector consists of a 6.3-cm × 6.3-cm NaI(Tl) crystal, read out with a photomultiplier tube (PMT) biased to 900 V. A spectrometer board developed by Lares Ltd. supplies the detector voltages with a 12 V input intended for power consumption under 25 W. The spectrometer is connected to a Windows 7 computer through Ethernet, and data are acquired with custom data acquisition (DAQ) software written by Lares Ltd. The detector was connected to a gas manifold (shown in Figure 2.1) at PNNL for the duration of the tests performed. The test procedure included the following tests, and the tests are described in the sections indicated in parentheses:

- physical stability testing (Section 3.1)
- quality assurance/quality check (QA/QC) measurements (Section 3.2)
- long-term gain stability testing (Section 3.3)
- spike measurements with ^{131m}Xe, ^{133}Xe, ^{133m}Xe, ^{135}Xe, and ^{222}Rn (Section 3.4)
- memory effect measurement (Section 3.5)
- comparison with another radioxenon detector (Section 3.6).

Figure 2.1. The Gas Manifold Used for Pressure Tests and Radioxenon Injection into the Silicon PIN Detector

3.0 Results

This section describes the results of the operation of the silicon PIN detector, which was tested along with plastic scintillator beta cells and a similar silicon PIN detector for comparison.

3.1 Physical Stability

The detector arrived from Russia in November 2013, and initial pressure tests were performed. The detector was capable of reaching a vacuum pressure of just under 1 torr. After replacing gas connections in an effort to resolve any leaks, the detector was able to reach a vacuum of 10^{-2} torr. Once pumping was stopped, the pressure slowly increased due to persistent leaks, reaching a pressure of approximately 40 torr in 30 minutes. For this reason, the calibration tests were performed immediately after pumping and at a pressure of approximately 1 atm in an effort to keep the radioxenon contained in the cell.

3.2 Quality Assurance/Quality Check Measurements

QA/QC measurements were performed periodically using a 0.5 μCi ^{137}Cs source. In Figure 3.1 the diagonal line is the coincidence for a Compton scatter event between the NaI and silicon PIN detector. The generation of an iodine X-ray within the NaI, which is subsequently detected within the silicon, is visible in the upper left corner of Figure 3.1.

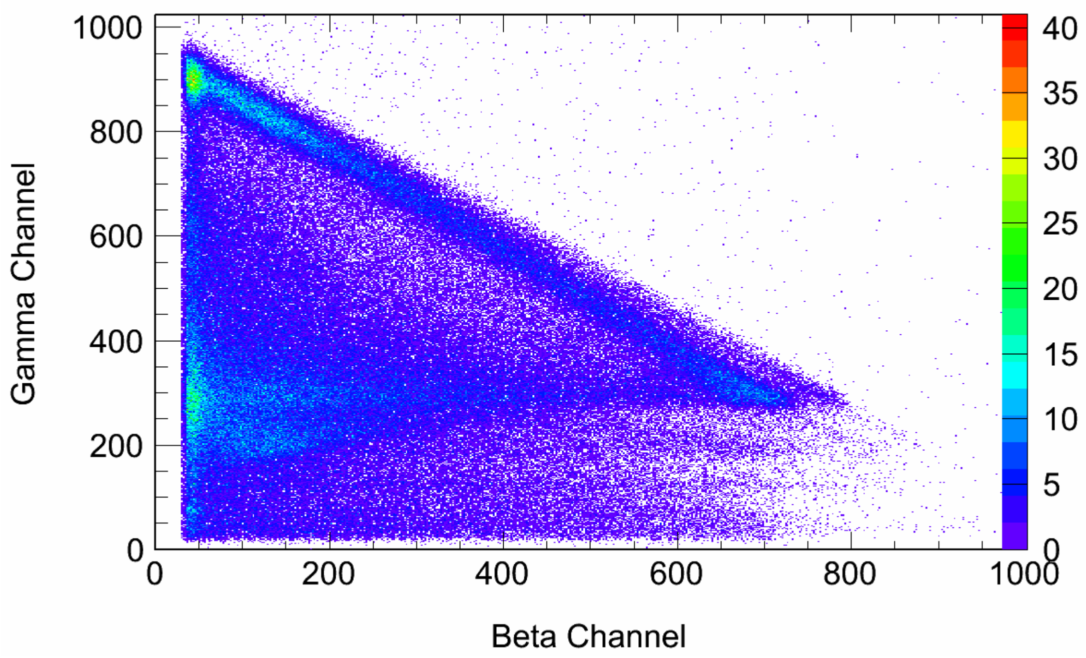

Figure 3.1. ^{137}Cs Beta-Gamma Coincidence Spectrum for the Silicon PIN Detector System. Detection of the iodine X-ray by the silicon is visible in the top left corner of the plot.

3.3 Long-term Gain Stability

To determine the long-term gain stability of both the silicon PIN detectors and the NaI detector, a ^{137}Cs QC run was taken periodically during a two-week period. Both the gain on the NaI detector and the silicon detector were stable over the course of gain measurements, as well as between system operations when the high voltage was completely turned off. Comparisons between runs are shown with the coincident gamma signal in Figure 3.2, and the coincident beta signal in Figure 3.3.

For the long calibration runs with ^{137}Cs, only the coincident events were saved to limit the size of the list-mode data files. In Figure 3.2, the Compton backscatter peak and the Compton edge line up very well among the three data sets. In the data set from 2014/03/20, the beta detector was able to reach a lower threshold allowing for the iodine X-ray to be observed, creating a larger number of events in the gamma coincidence spectra (channel 220). For the beta spectra in Figure 3.3, the uniform shape and end-points of the beta spectra show that the silicon detector gain was very stable over the course of data taking. In the data set from 2014/03/20, the beta detector was able to reach a lower threshold allowing for the iodine X-ray peak to be observed at about channel 15.

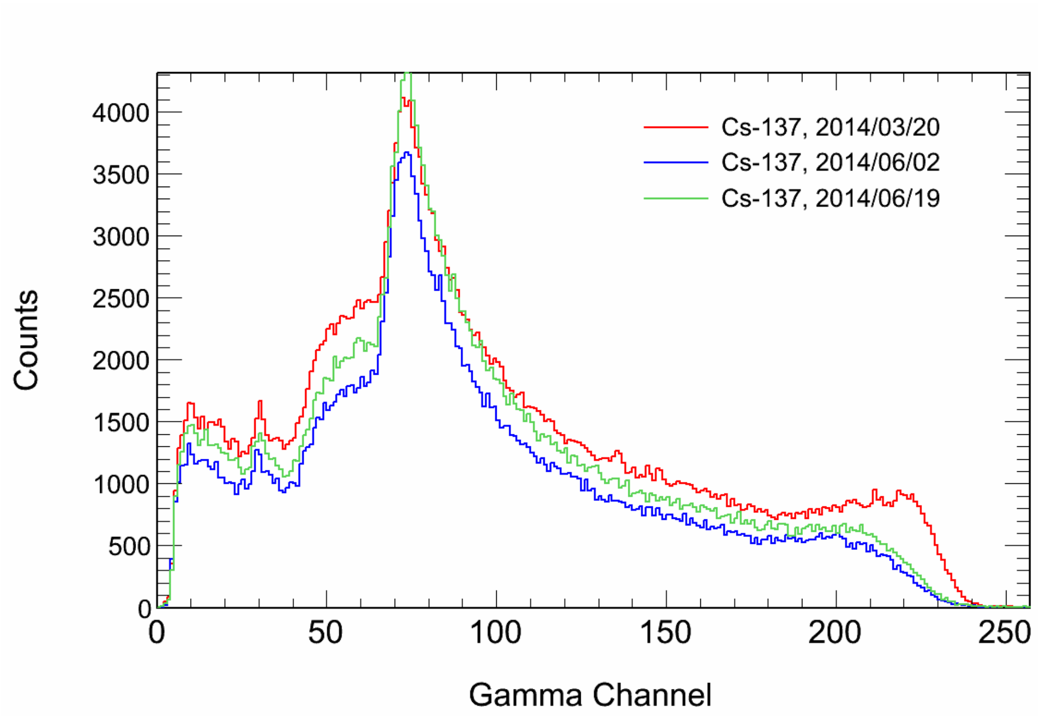

Figure 3.2. Coincident Gamma Spectra for the Start and End of the ^{137}Cs gain tests, on 2014/06/02 and 2014/06/19, Along with a Previous Data Set from 2014/03/20. The gain stability for the NaI detector was very good both during the gain stability testing and compared to previous data.

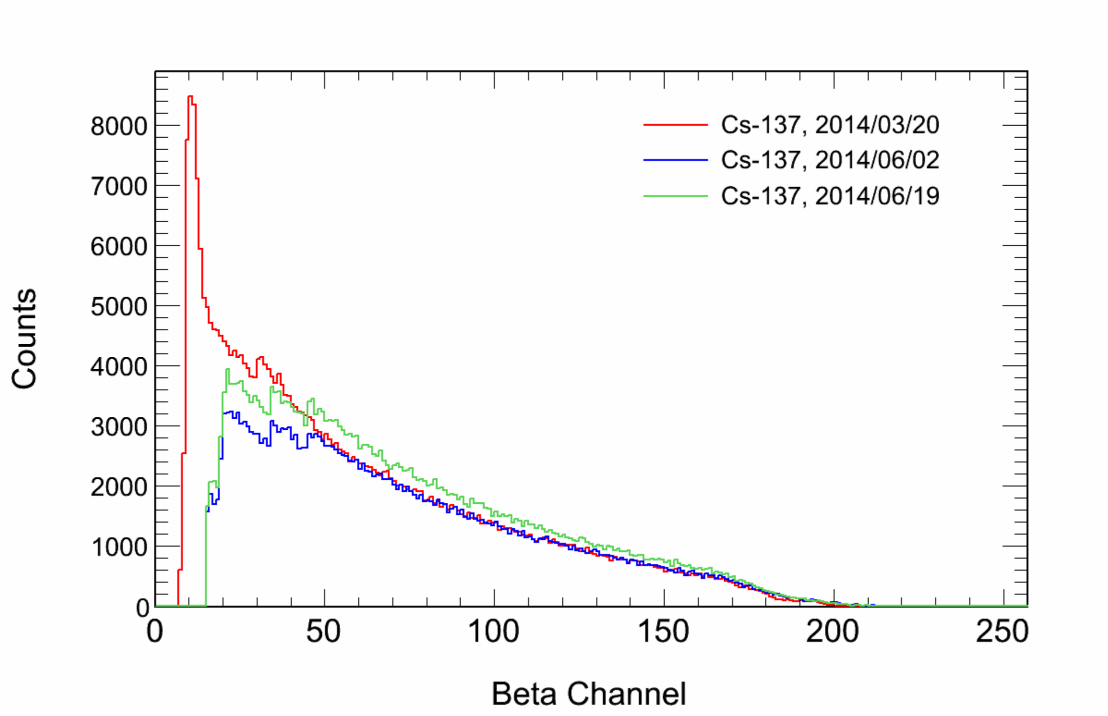

Figure 3.3. Coincident Beta Spectra for the Start and End of the Gain Tests 2014/06/02 and 2014/06/19, Along with a Previous Data Set from 2014/03/20

3.4 Xenon Spike Measurements

Xenon spikes were used for detector testing and calibration. Because of the high event rate in each of these samples, summing "shadows" are visible at the gamma channels above the primary bands (see Figures 3.4 through 3.8). The figures for the ^{222}Rn and ^{131m}Xe spikes are shown in Section 3.5 for the memory effect tests. The effect of the low-energy noise present in the beta spectra results in the inability to perform a complete detector calibration.

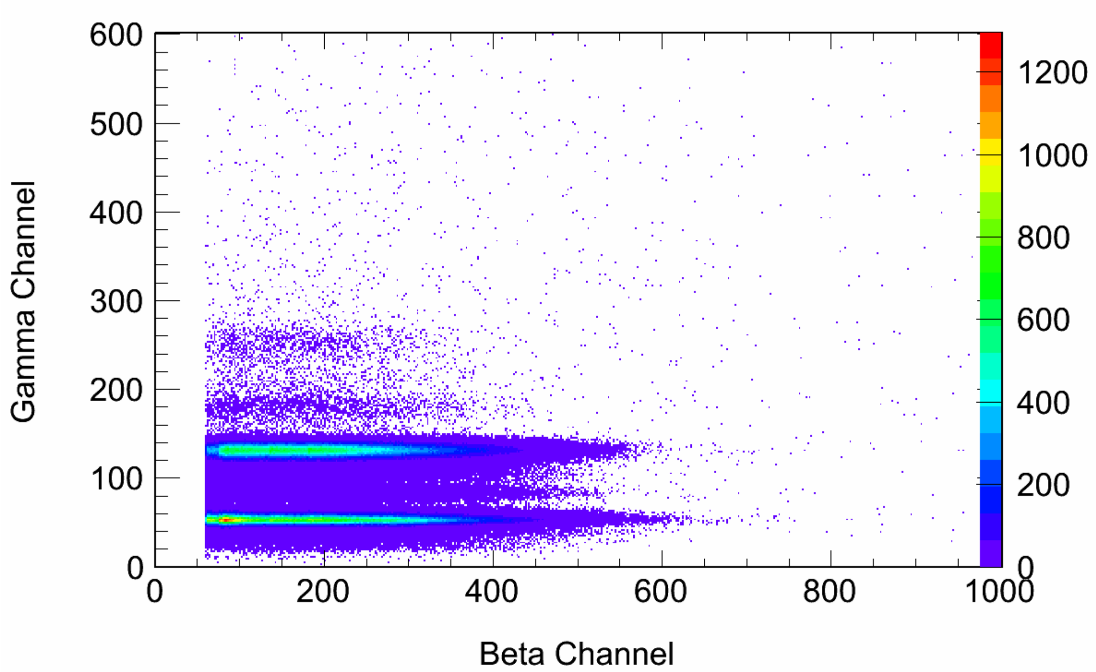

Figure 3.4. ^{133}Xe Spike, Counted for 18 Hours with the 45-keV Conversion Electron Peak Visible at a Beta Channel of about 80. The noise variability at low beta energies because of the Si PIN threshold effects is visible as slight discontinuities in the 80-keV band (beta channels 50-100).

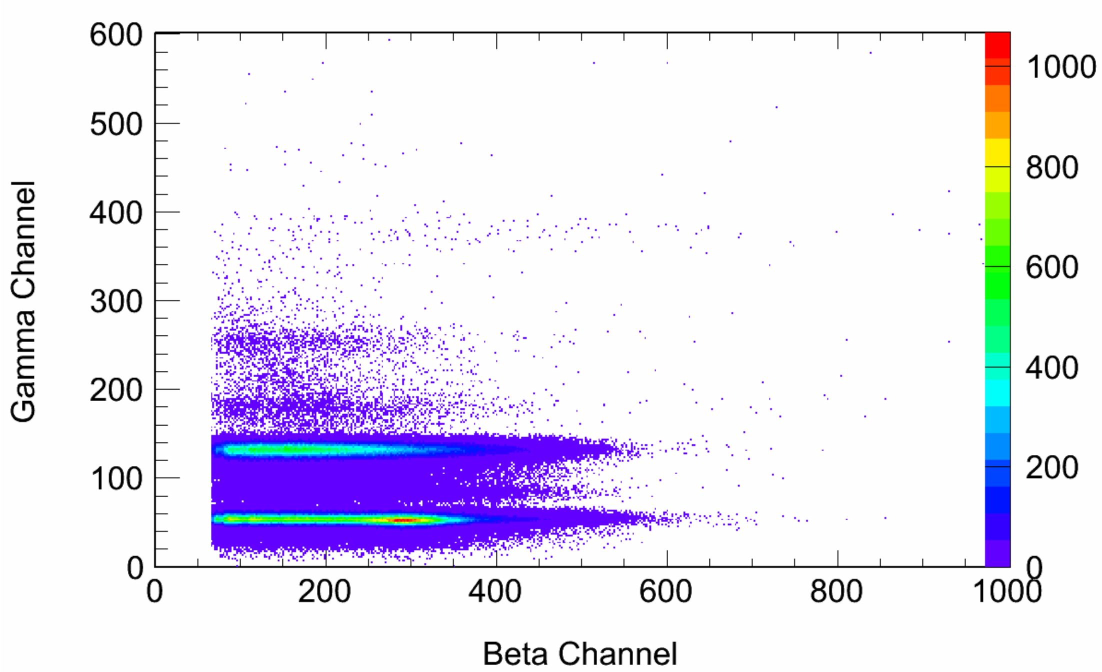

Figure 3.5. ^{133m}Xe Spike, Counted for 18 Hours with the Similar ^{133}Xe Structure as in Figure 3.4, but with the Peak at Channel 300 because of the ^{133m}Xe Conversion Electron Peak

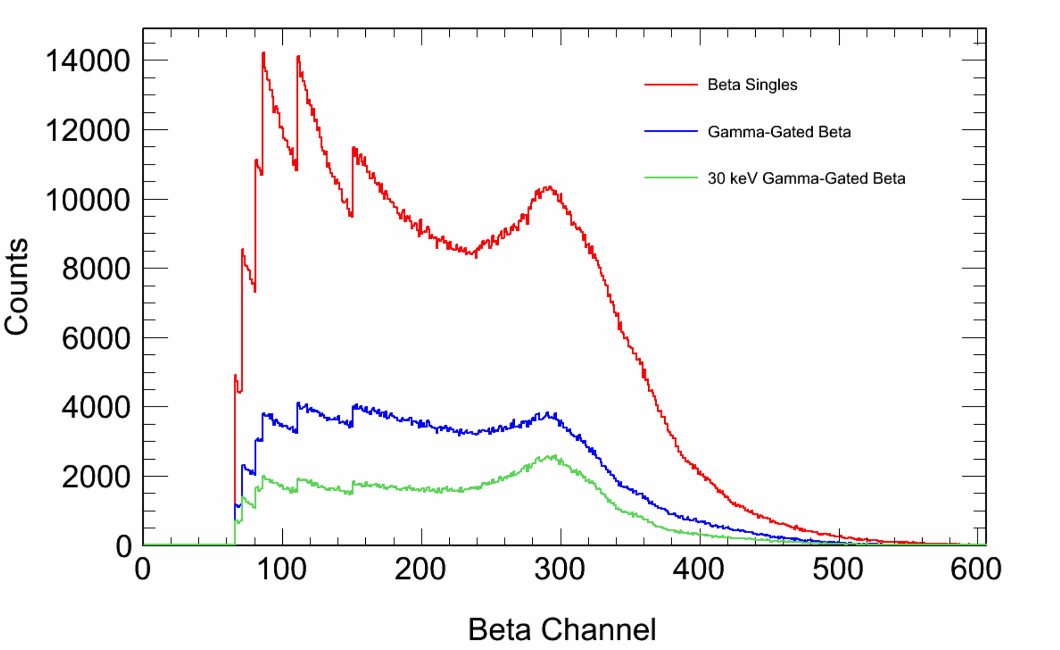

Figure 3.6. ^{133m}Xe Spike, Counted for 18 Hours. The beta singles spectrum (red) has a large component of the low-energy noise, but the ^{133m}Xe peak is still distinguishable from the ^{133}Xe background. The gamma-gated betas (blue) reduce the low-energy noise; further gating on only the 30-keV X-ray (green) reduces the ^{133}Xe background and increases the signal to background of the ^{133m}Xe.

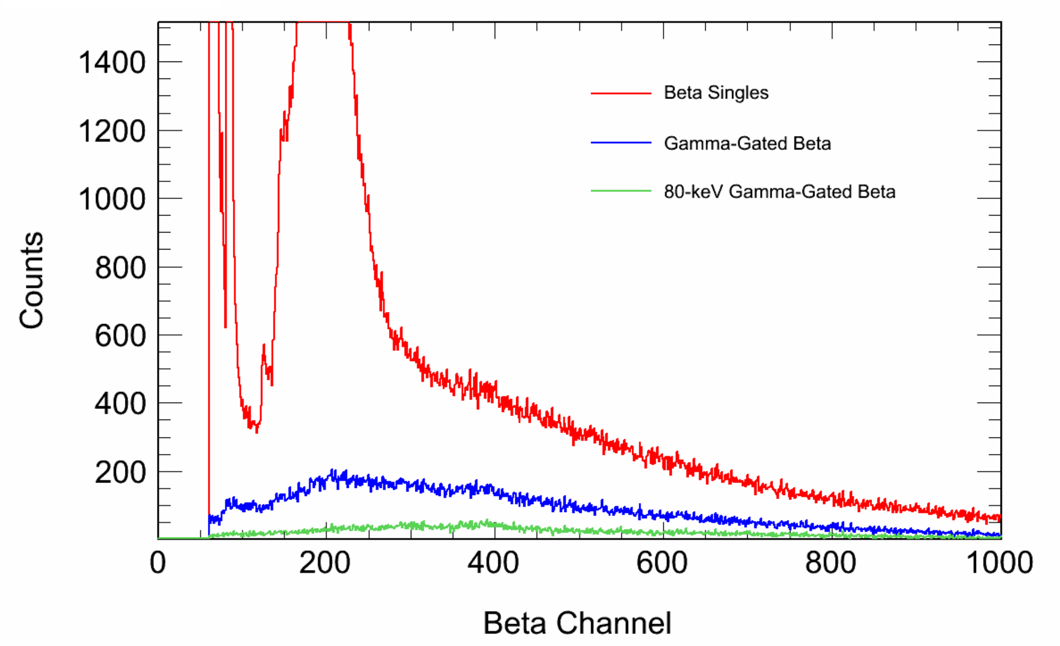

Figure 3.7. ^{222}Rn Spike, Counted for 24 Hours. The low-energy noise of the different silicon channels has a large effect on the beta singles spectrum, while the gamma-gated signal produces a cleaner spectrum. The 80-keV gamma-gated spectrum peaks at a higher energy, in agreement with the ^{222}Rn decay scheme.

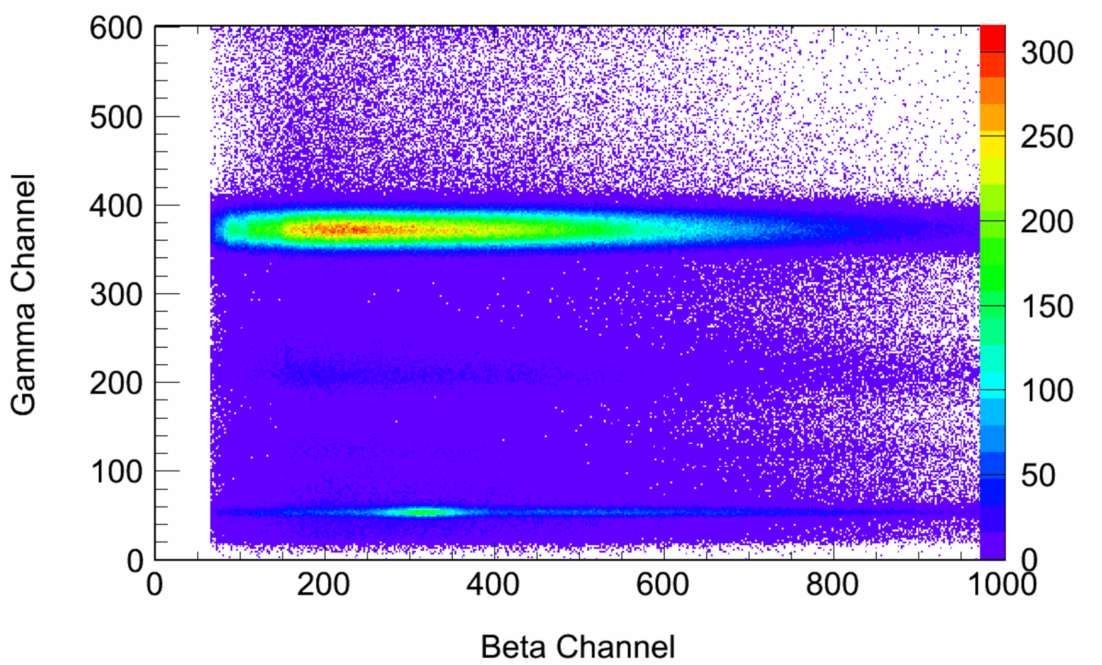

Figure 3.8. ^{135}Xe Spike, Counted for 18 Hours, Showing Primarily the ^{135}Xe with a Small Fraction of ^{133}Xe and ^{133m}Xe Present

3.5 Memory Effect Measurements

The memory effect was measured using a ^{131m}Xe spike. The calibration spike was counted in the detector for 18 hours (Figure 3.9) followed by a pump and flush of the detector and an 18-hour gas background measurement (Figure 3.10). A small amount of ^{133}Xe was visible within the ^{131m}Xe spike. The count rate of the ^{131m}Xe spike was 4.45 events/second, while the gas background data showed an event rate of 0.02 events/second for a memory effect of about 0.5 percent. It is believed that the primary source of the memory effect is the plastic housing that holds the silicon PIN diodes to make the beta cell. A similar test was performed for an ^{222}Rn spike, but with a detector count time for 24 hours, measuring a memory effect of about 6 percent (Figure 3.11). Because these measurements are close, the primary source of the memory effect was the ^{214}Pb present from the radon spike, which could not be pumped out. With sufficient time for the ^{214}Pb to decay away ($t_{½}$ = 29 min.) between measurements, the memory effect would more closely resemble that of ^{131m}Xe (Figure 3.12).

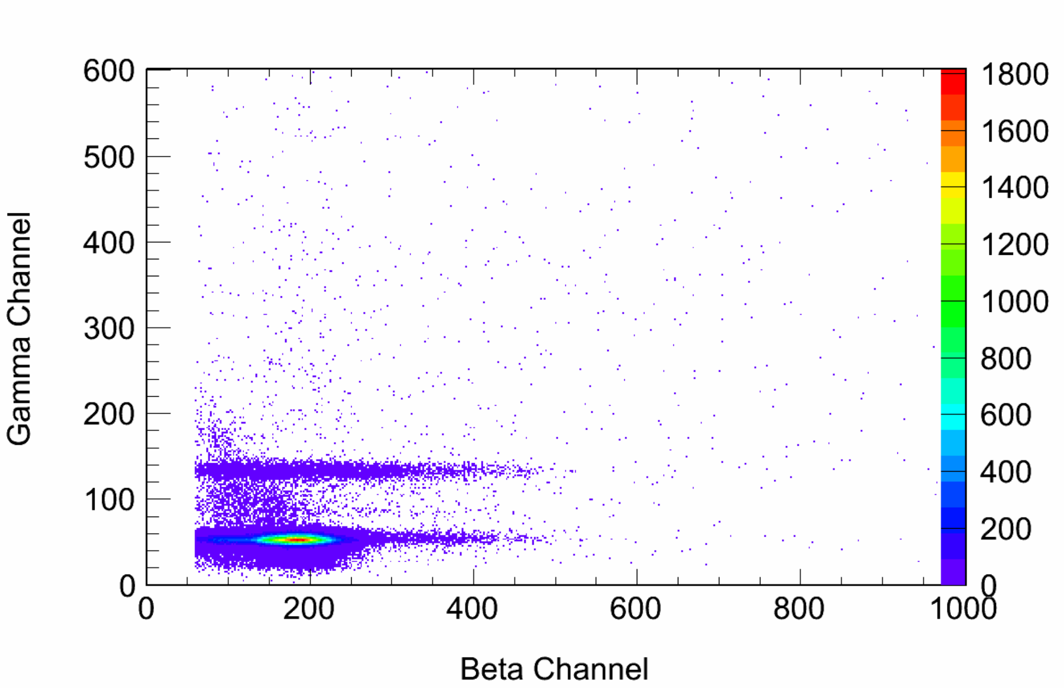

Figure 3.9. ^{131m}Xe spike Counted for 18 Hours to Measure the Memory Effect of the Silicon PIN Detector, with an Event Rate of 4.45 Events/Second

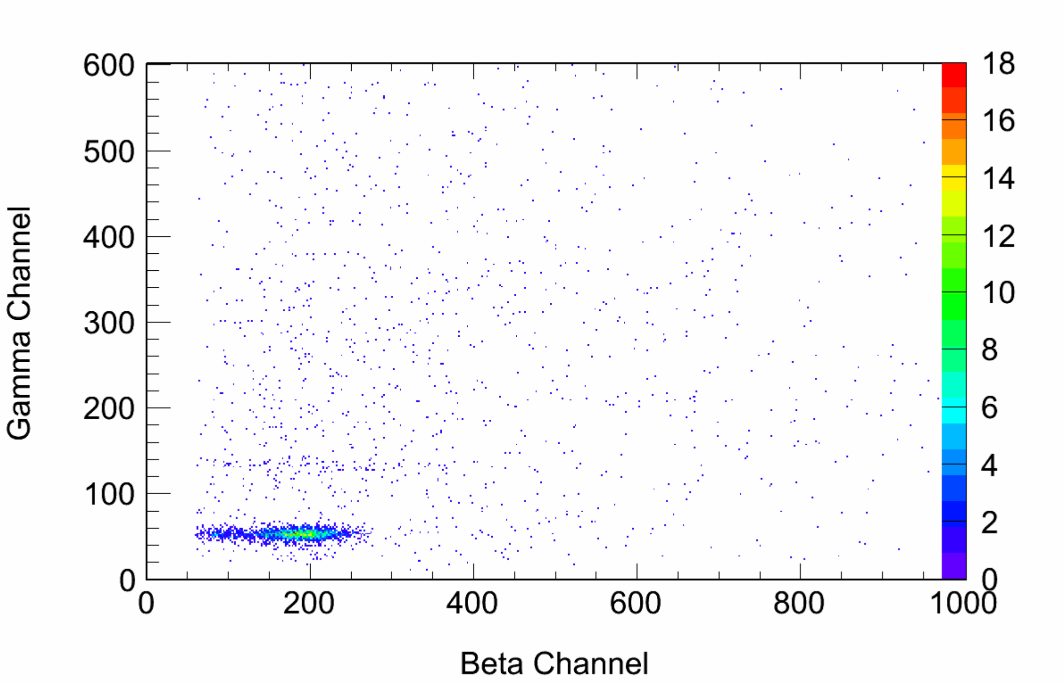

Figure 3.10. ^{131m}Xe Gas Background Run After the ^{131m}Xe Spike, Measuring an Event Rate of 0.02 Events/Second for a Memory Effect of about 0.5 Percent

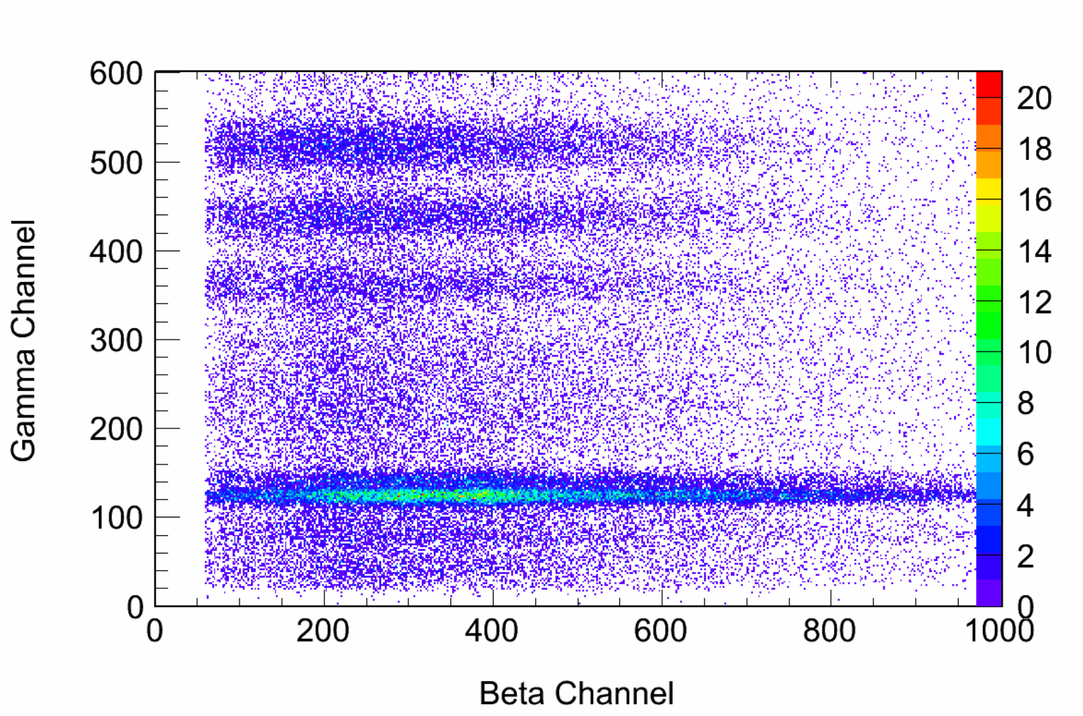

Figure 3.11. Radon Spike Counted for 24 Hours to Measure the Radon Memory Effect of the Silicon PIN Detector

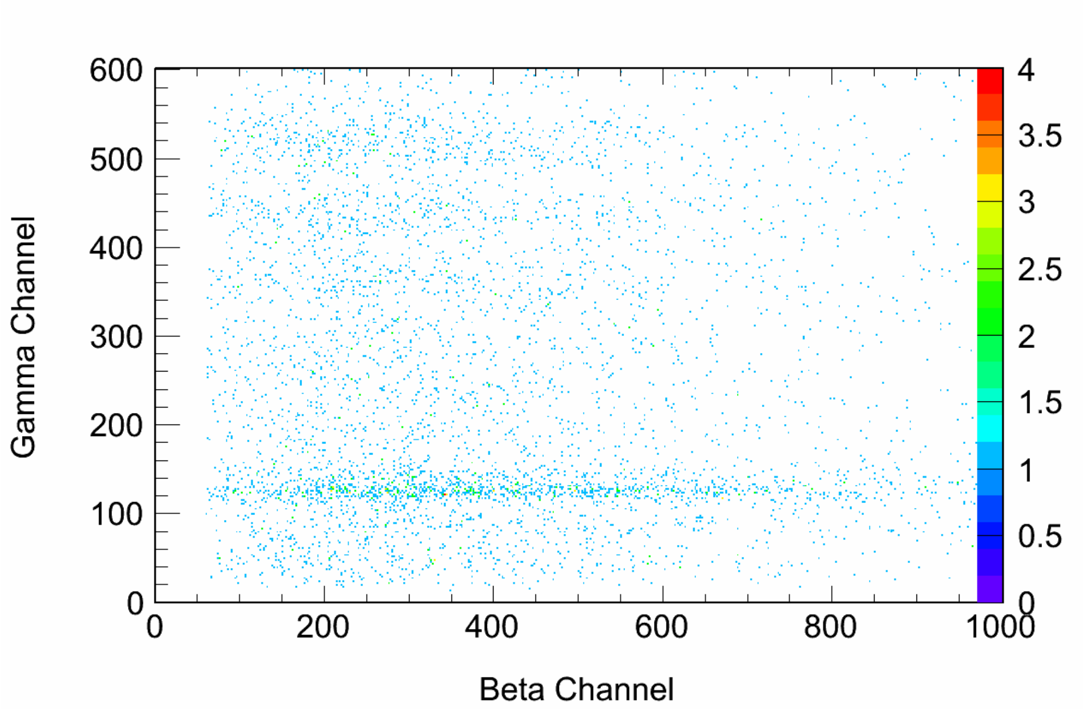

Figure 3.12. Radon Gas Background Measured Immediately Following the ^{222}Rn Spike, with a Memory Effect of about 6 Percent. The primary memory effect source was the decay of the ^{214}Pb from the spike measurement that was left in the cell after pumping.

3.6 Comparison with Plastic Scintillator

The low-energy noise made a representative detector comparison difficult for two reasons:

- The high threshold resulted in the loss of low-energy signals, which are beneficial to radioxenon detection.
- The variability in the noise resulted in a decreased energy resolution compared to previous measurements.

Given these shortcomings, comparisons to both a current-generation plastic scintillator beta cell and a silicon PIN detector of the same model from Lares Ltd. were performed.

The two primary benefits of a silicon beta cell are decreased memory effect, and increased resolution.

3.6.1 Decreased Memory Effect

The first benefit of a silicon beta cell is decreased memory effect. Current generation plastic scintillator beta cells show a xenon memory effect of about 5.0 percent (McIntyre et al. 2001). Silicon reduced the memory effect dramatically as expected, to 0.5 percent, but there is potential for the memory effect to be reduced even further. Currently the plastic housing accounts for approximately one third of the surface area of the beta cell material; if the plastic housing for the silicon detectors is reduced, the memory effect will likely be decreased even further.

3.6.2 Improved Resolution

The second benefit of silicon beta cells is increased resolution compared to plastic scintillators. For the ^{131m}Xe 129-keV conversion electrons, a standard resolution in a plastic scintillator cell is about 30 percent full width at half maximum (FWHM). Because of the high and varying thresholds for each of the silicon channels, the resolution of the silicon detector tested suffered. The measured detector resolution for the silicon detector tested was about 30 percent as well, but this was much worse than similar silicon detectors that do not suffer from the high threshold. One example of a similar detector is a silicon detector of the same Lares Ltd. model tested in Russia (Popov 2013). For this detector, the resolution was under 10 percent FWHM. At under 10 percent resolution, separation of the conversion electrons is achieved (see Figure 3.13), and better identification of the metastable isotopes within a ^{133}Xe background is possible (Figure 3.14). A comparison between the PNNL-tested silicon detector and a similar model tested at Lares Ltd. is shown in Figure 3.15. The PNNL detector exhibited a response much more similar to the scintillator beta cell than to the silicon beta cell tested at Lares Ltd. The effect of the low-energy noise was also visible in the PNNL data, while the spectrum from Lares Ltd. showed no low-energy noise issue.

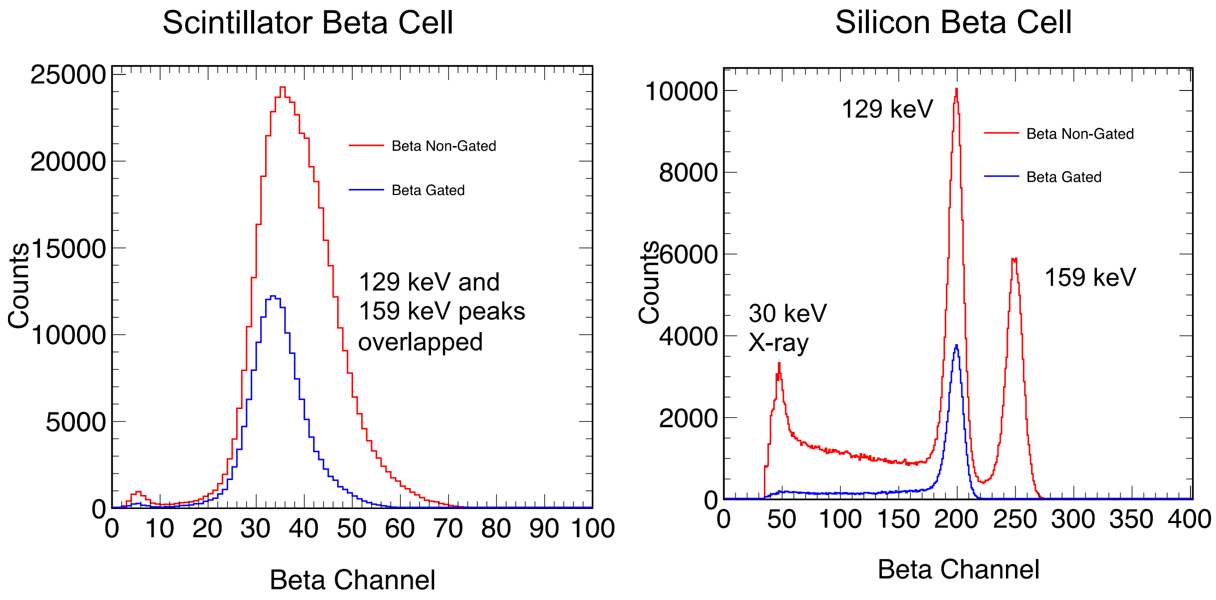

Figure 3.13. Beta Singles Spectra (red) and Gamma-gated Beta Spectra (blue) for the Plastic Scintillator (left) and the Lares Ltd.-tested Si Detector (right). The silicon PIN diode detector's increased resolution allows the two ^{131m}Xe conversion electrons (129 keV and 160 keV) to be distinguished.

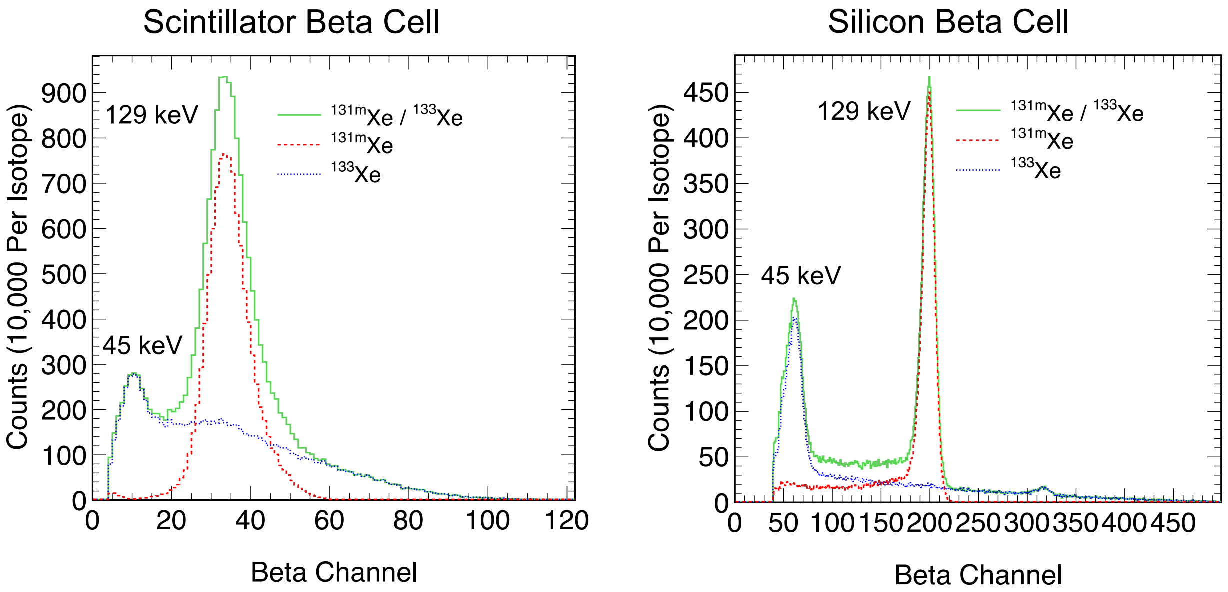

Figure 3.14. Plastic Scintillator (left) and Silicon (right) Data for ^{131m}Xe (red), ^{133}Xe (blue), and a Software Combined ^{131m}Xe and ^{133}Xe (green) Data Set. The silicon PIN detector's increased resolution renders the xenon isomers more easily identified in a ^{133}Xe background. A small fraction of ^{133m}Xe present in the silicon ^{133}Xe sample produced the small hump near channel 300. The silicon detector data were provided by Lares Ltd. for the system they tested.

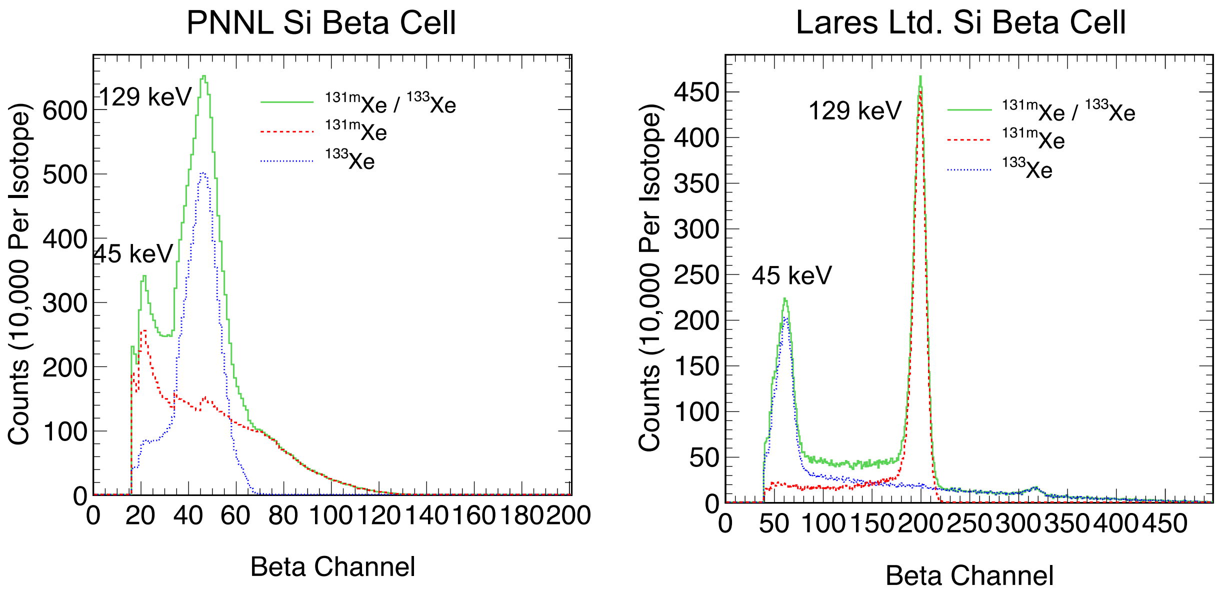

Figure 3.15. A Comparison of the PNNL-tested Silicon Detector (left) with the Lares Ltd.-tested Detector (right) for ^{131m}Xe (red), ^{133}Xe (blue), and a Software Combined ^{131m}Xe and ^{133}Xe (green) Data Set. Note: The beta channel scales are different for these two plots. The data for the PNNL silicon beta cell (left) were for 256 bins, while the Lares Ltd. data (right) were for 1024 bins.

3.7 Multiplicity Analysis

With the ability to detect coincidence events within the beta cell, additional nuclear physics can be explored. ^{133}Xe produces a triple coincidence event with an emission of a conversion electron, X-ray, and beta particle. The detection of the three particles in coincidence is a clear sign of ^{133}Xe decay within the detector. In order to detect triple coincidence events, the silicon PIN diodes must be capable of distinguishing between the conversion electron and beta particle. The capability of the silicon PIN diodes to detect events with a multiplicity greater than one is studied in this section.

With data taken in list-mode in addition to pulse-height data (PHD) files, it is possible to analyze the beta signals on a channel-by-channel basis and observe the multiplicity of beta hits within the cell. Outside backgrounds may be directional and therefore have a different multiplicity than the internal signals. One example of this could be cosmic rays traversing the detector from top to bottom. For a mixed gas sample, there was no observable difference in the multiplicity of beta events between beta singles and betas coincident with a gamma ray (see Figures 3.16 and 3.17). Another method of inspecting the beta signals is to plot the beta energy from one side of the silicon cube versus another. Figure 3.18 is such a plot for beta singles, and Figure 3.19 is the plot for gamma-gated betas.

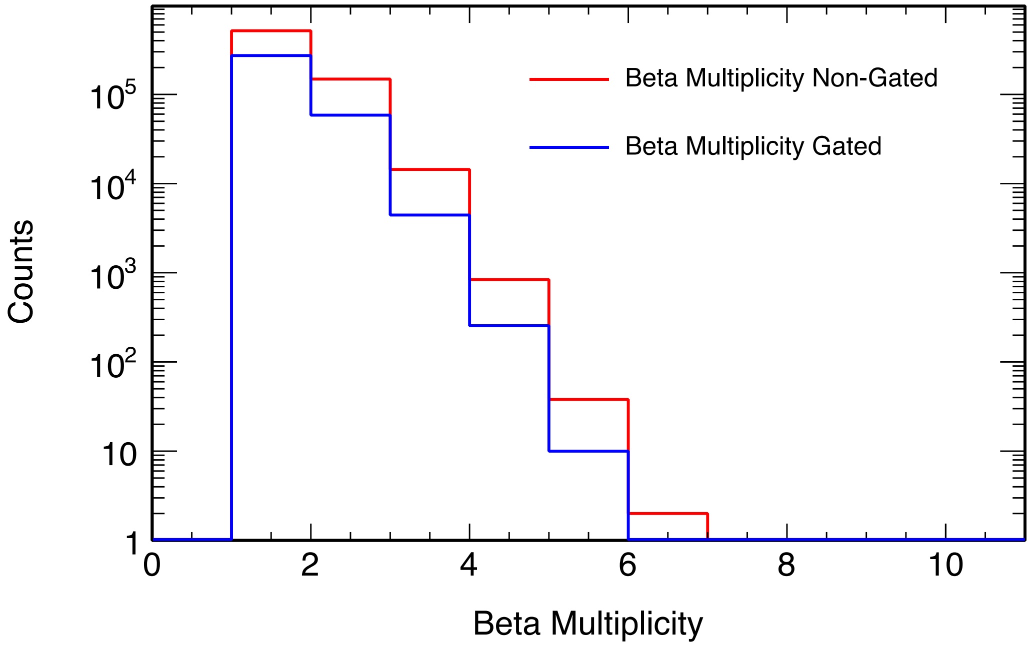

Figure 3.16. Multiplicity of Beta Singles Across the Six Silicon PIN Detectors, which make up the Beta Cell for a ^{135}Xe, ^{133}Xe, and ^{133m}Xe Spike

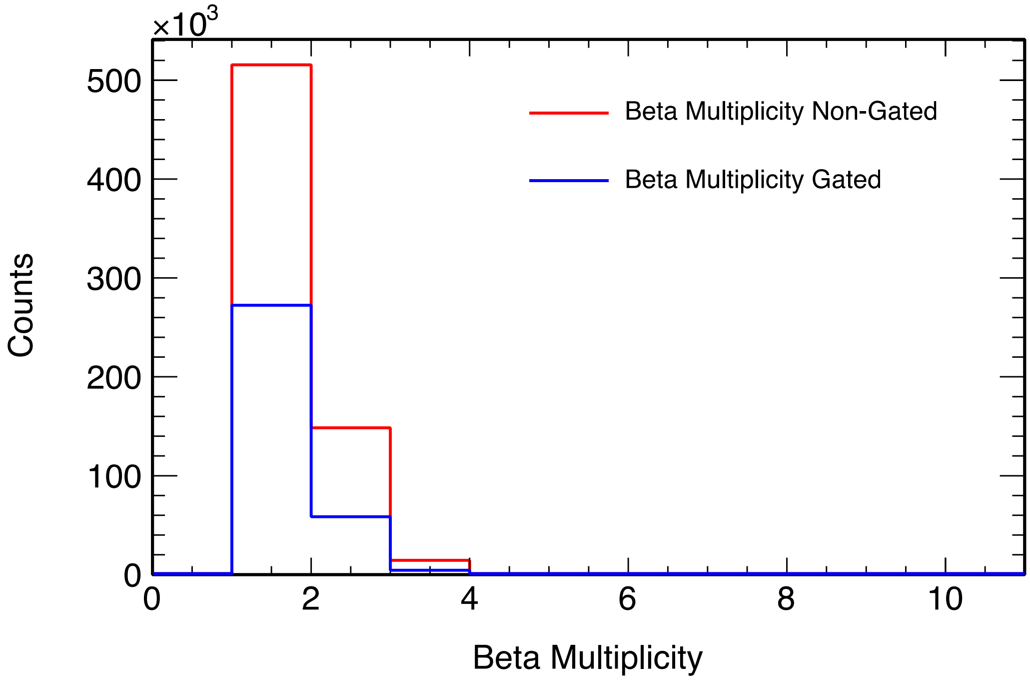

Figure 3.17. Multiplicity Across the Six Silicon PIN Detectors of Beta Events, which are Coincident with a Gamma Event for a ^{135}Xe, ^{133}Xe, and ^{133m}Xe Spike

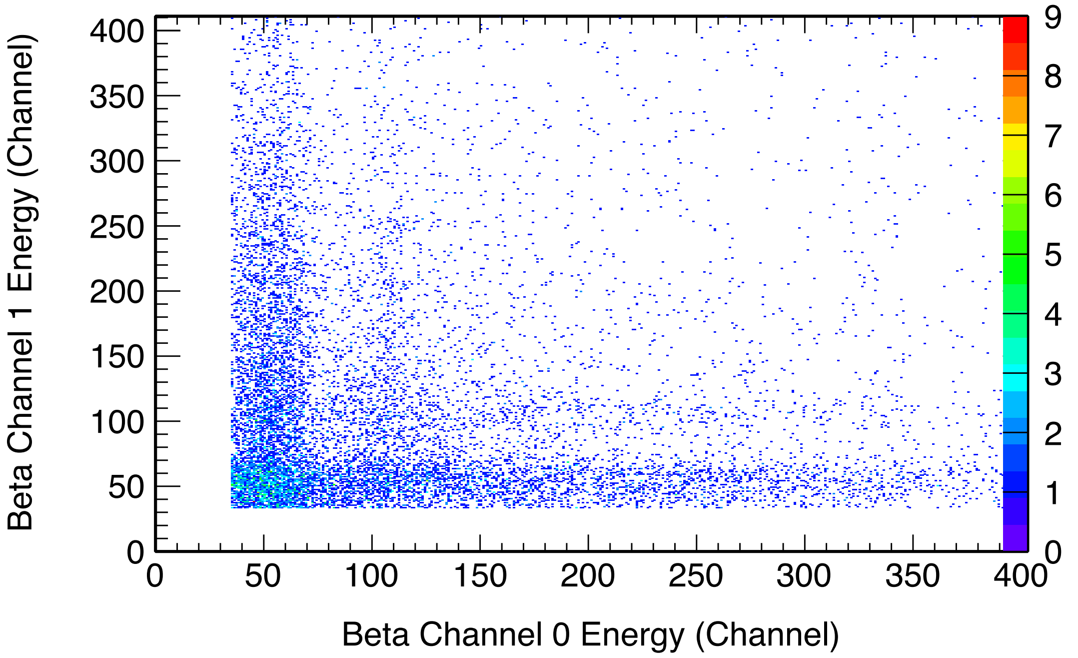

Figure 3.18. Energy Detected by Side 1 of the Silicon Cell Versus Side 2 of the Cell for a ^{135}Xe, ^{133}Xe, and ^{133m}Xe Spike. The 30-keV lines are clearly visible, along with the lines created by the 80-keV X-ray.

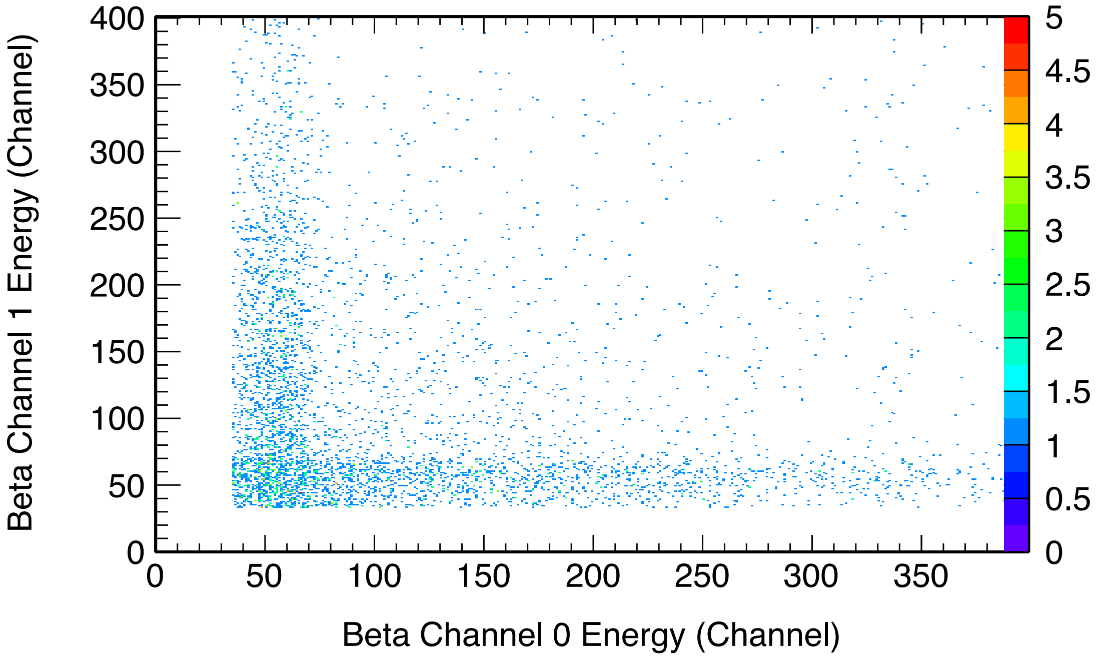

Figure 3.19. Energy Detected by Side 1 of the Silicon Cell Versus Side 2 for a ^{135}Xe, ^{133}Xe, and ^{133m}Xe Spike. The 30-keV lines are clearly visible. As expected based on the gated beta spectrum, the lines created by the 80-keV X-ray are not present when a gamma coincidence is required.

Another useful representation of the silicon data is a plot of the most energetic event detected by the silicon detectors versus the second-most energetic event they detect, Figure 3.20. The detection of beta particles across the silicon detectors creates a triangle in the lower left portion of the plot. When an event of discrete energy is detected such as that of an X-ray or conversion electron, horizontal and vertical lines are produced within the plot. The horizontal and vertical lines meet at the point of the X-ray or electron energy along the y=x line. From this point, event sets in which the discrete event is more energetic produces a vertical line downward. The horizontal line moving in the positive energy direction is generated for instances in which the X-ray event generates a smaller signal than that of the beta particle. A triple coincidence event is visible in Figure 3.20 as a horizontal and vertical line meet at the point along the y=x line of the conversion electron energy.

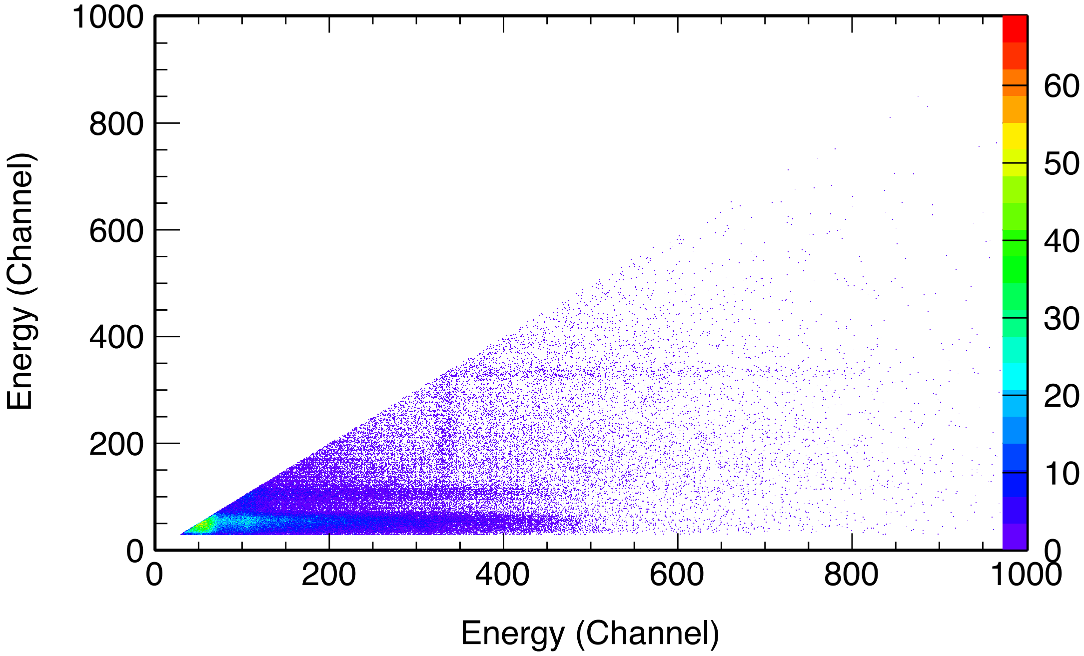

Figure 3.20. Silicon Detector Data for a ^{135}Xe, ^{133}Xe, and ^{133m}Xe Spike. The most energetic event detected by the six silicon detectors is plotted on the x axis, and the second-most energetic event detected on any of the six silicon detectors is plotted on the y axis. The beta particles create the uniform scatter of points throughout the triangle, while the detection of an electron capture electron creates the horizontal and vertical lines.

3.8 Electron Backscatter Signals

Multichannel silicon analysis allows for the investigation into electron backscatter signals. Because of the higher atomic mass of the silicon compared to that of scintillator plastic, there is an increased electron backscatter signal. This is especially visible in the ^{131m}Xe data Figure 3.21 in which the 129-keV conversion electrons also produce a low-energy electron backscatter tail. Multichannel events could be attributed to two possible sources:

- triple coincidence events
- electron backscatter along with primary electron signal.

The primary source of multichannel events is determined to primarily be electron backscatter from the presence of the signal in all isotopes and energy spectrum of the events. To reduce the effect of electron backscattering, all silicon hits in a coincidence window are summed together to create one silicon event (Figure 3.21). This is also a good case to demonstrate the efficacy of using a silicon detector as a modular replacement for plastic scintillator beta cells that only have one channel. In this instance, all six silicon channels would be physically summed and input into a current radioxenon system. A beta coincidence matrix was put together to determine any trends in the coincidence between the beta signals (Figure 3.22). This analysis shows that the action of physically combining all the silicon channels will not detract from the potential of the silicon PIN detector to yield the benefits stated in Section 3.6.

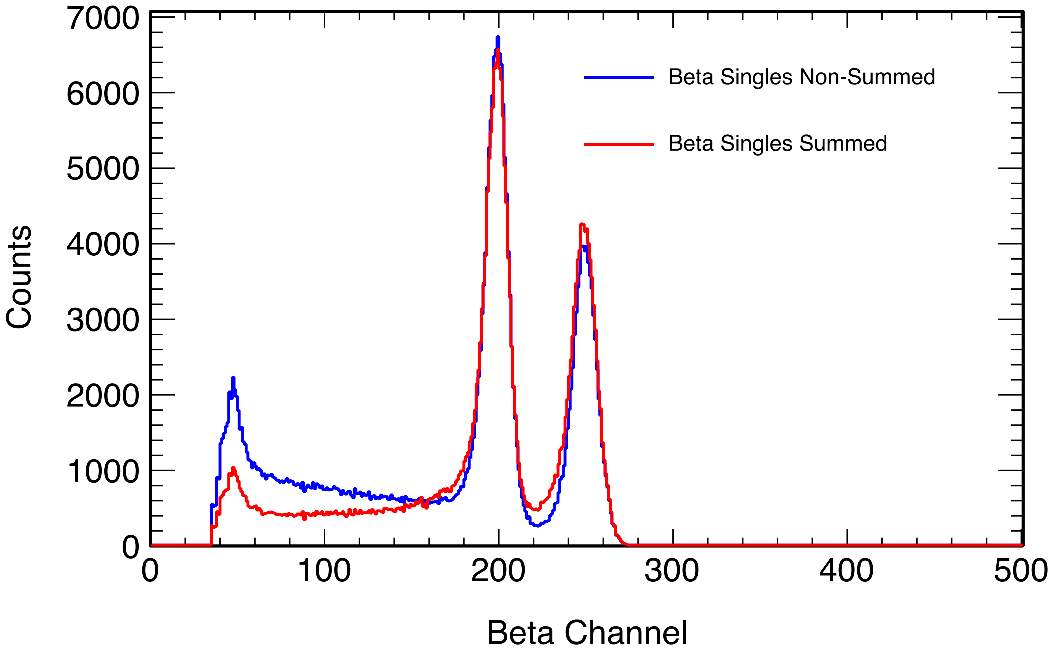

Figure 3.21. ^{131m}Xe Beta Signal Showing the Low-energy Electron Backscatter Tail in Addition to the 129-keV and 159-keV Conversion Electron Peaks. Data shown are from Lares Ltd. for a better view of the electron backscatter tail. The low-energy peak at beta channel 50 is because of detection of the 30-keV X-rays.

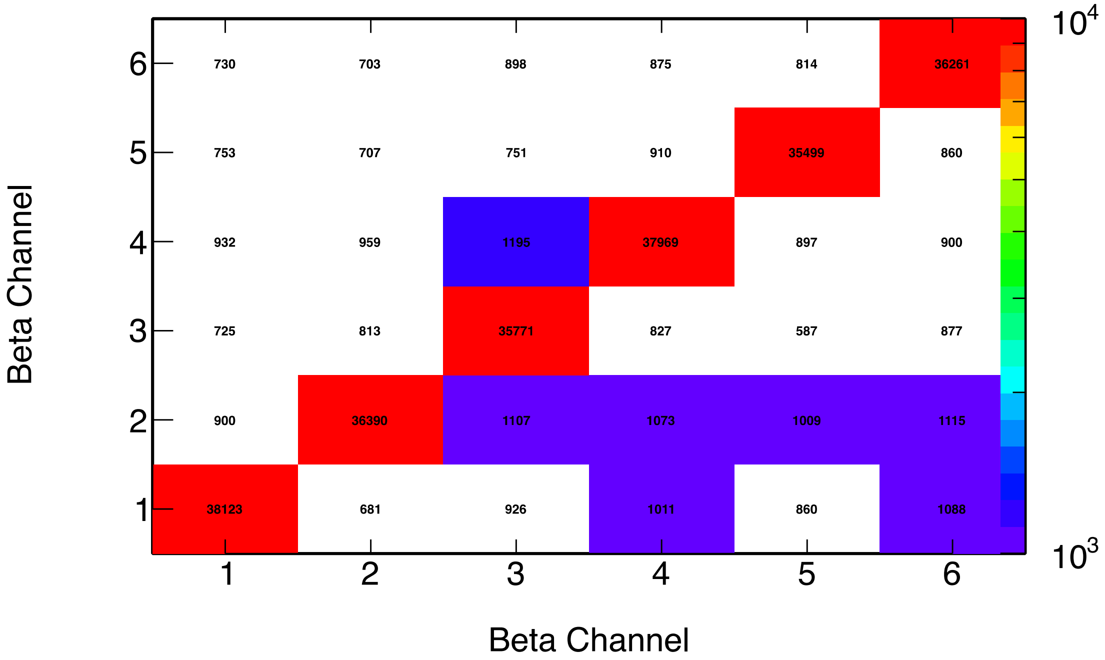

Figure 3.22. Beta Coincidence Matrix Showing a Uniform Event Rate of Single Channel Events and a Uniform Distribution of the Multichannel Events Across all Channels. The center x=y line (red boxes) corresponds to single channel events, and the other boxes represent the number of times channel y had a hit when channel x was the first to trigger.

4.0 Conclusions

This section covers conclusions about primary detector limitations; minimum detectable concentration (MDC); demonstrated benefits, improvements, and efficacies; and next steps.

4.1 Primary Detector Limitations

There were two primary limitations to the silicon PIN detector tested at PNNL, but both limitations should be capable of being addressed in future iterations. The first limitation, which had the largest effect on the data, and was low-energy noise that required the threshold be increased to the point of losing some low-energy signals. The second limitation, experienced at PNNL, was the presence of a small leak somewhere in the gas chamber, which reduced the ability to operate the detector in the manner required for the IMS.

4.1.1 Noise

Each silicon PIN detector channel experienced a varying degree of noise. With the noise present, the event rate was beyond the capabilities of the DAQ software, and the lower-level discriminator had to be set high enough to cut out the low-energy noise. The relatively high threshold, between 30 and 100 keV depending on the channel, had a few impacts on the system:

- The higher threshold resulted in missing out on the lower-energy beta signals, skewing the detector efficiency.
- With the high thresholds and the noise creeping above the threshold for portions of the run, the resolution was greatly diminished.
- The high rate of noise could cause potential false coincidence events, as evidenced in Figure 3.3.

4.1.2 Pressure Leak

The other issues hampering the operation of the silicon detector were its lack of physical stability and the gas leak that initially prevented vacuum in the detector (see Section 3.1). While this was a problem for the operation of the detector at PNNL, it should be mitigated easily in any future development of the silicon detector model.

4.2 Minimum Detectable Concentration

Along with the limitations presented in Section 4.1, a representative calibration and MDC calculation could not be performed. For the discussion of MDCs, we used the results from the Lares Ltd.-operated silicon detector. Assuming 1 cm^3 of xenon in laboratory-like conditions, and a 24-hour count time (12-hour count time for the SAUNA), the MDCs for the silicon detector tested by Lares Ltd. (and a conventional SAUNA system) were calculated to be

- ^{131m}Xe – 0.12 mBq/m^3 (0.12 mBq/m^3)
- ^{133}Xe – 0.18 mBq/m^3 (0.21 mBq/m^3)
- ^{133m}Xe – 0.07 mBq/m^3 (0.15 mBq/m^3)
- ^{135}Xe – 0.45 mBq/m^3 (0.67 mBq/m^3)

The MDC for the xenon isomers are about 20 to 35 percent lower than those of a SAUNA detector (Hennig et al. 2013) for a 12-hour count, while those for ^{133}Xe and ^{135}Xe are equivalent. In order to reduce the MDCs for the silicon detector, the plastic housing that holds the silicon PIN diodes must be minimized. In reducing the plastic housing, the solid angle covered by the PIN diodes increases, which increases the beta detection efficiency.

4.3 Demonstrated Benefits/Improvements/Efficacies

In spite of observed limitations and room for improvement, this technology shows a great deal of promise in improving the precision with which detectors can distinguish various xenon isotopes in the future, benefitting the CTBTO’s IMS operations greatly. The ability of the silicon beta cell to separate the metastable xenon isotopes from the ^{133}Xe background, will aid in the characterization of detected radioxenon events. With a decreased surface area of the silicon PIN diode housing, the memory effect and MDCs have the potential to be further reduced, improving the operation of the silicon detector.

4.4 Next Steps

In order for a silicon detector to be a modular replacement for current plastic scintillator cells, research needs to be performed into the development of a robust and reliable system. A field system incorporating a silicon beta cell must have a stable and low noise threshold in order to have uniform detection efficiency. Work is required to determine the optimal silicon detector size, aspect ratio, and thickness, along with a method of packing the diodes in a manner that allows for increased solid angle coverage and detection efficiency. In addition to development on the silicon beta cell, a means of integration into a current detection system is required. Two integration examples are providing each diode with the required high voltage and reading out each of the signal paths into the current or compatible DAQ system.

5.0 References

Cagniant A, G Le Petit, P Gross, G Douysset, H Richard-Bressand, and JP Fontaine. 2014. "Improvements of Low-Level Radioxenon Detection Sensitivity by a State-of-the Art Coincidence Setup." *Applied Radiation and Isotopes*, 87:48-52. DOI 10.1016/j.apradiso.2013.11.078.

Hennig W, CE Cox, SJ Asztalos, H Tan, PJ Franz, PM Grudberg, WK Warburton, and A Huber. 2013. "Study of Silicon Detectors for High Resolution Radioxenon Measurements." *Journal of Radioanalytical and Nuclear Chemistry,* 296(2):675-81. DOI 10.1007/s10967-012-2053-y.

Le Petit G, A Cagniant, M Morelle, P Gross, P Achim, G Douysset, T Taffary, and C Moulin. 2013. "Innovative Concept for a Major Breakthrough in Atmospheric Radioactive Xenon Detection for Nuclear Explosion Monitoring." *Journal of Radioanalytical and Nuclear Chemistry,* 298(2):1159-69. DOI 10.1007/s10967-013-2525-8.

McIntyre JI, KH Abel, TW Bowyer, JC Hayes, TR Heimbigner, ME Panisko, PL Reeder, and RC Thompson. 2001. "Measurements of Ambient Radioxenon Levels Using the Automated Radioxenon Sampler/Analyzer (ARSA)." *Journal of Radioanalytical and Nuclear Chemistry,* 248(3):629-35. DOI 10.1023/a:1010672107749.

Popov V. 2013. "Beta-Gamma Coincidence Spectrometer with Si PIN Diodes." Presented at International Noble Gas Experiment Workshop, November 4-8, 2013, IAEA, Vienna, Austria.

Schroettner T, I Schraick, T Furch, and P Kindl. 2010. "A High-Resolution, Multi-Parameter, Beta-Gamma Coincidence, Mu-Gamma Anticoincidence System for Radioxenon Measurement." *Nuclear Instruments & Methods in Physics Research Section A-Accelerators Spectrometers Detectors and Associated Equipment,* 621(1-3):478-88. DOI 10.1016/j.nima.2010.06.227.

Pacific Northwest
NATIONAL LABORATORY

U.S. DEPARTMENT OF
ENERGY

Proudly Operated by Battelle *Since 1965*

902 Battelle Boulevard
P.O. Box 999
Richland, WA 99352
1-888-375-PNNL (7665)

www.pnnl.gov